THE ORIGIN OF SHORT-LIVED RADIONUCLIDES AND EARLY SOLAR SYSTEM IRRADIATION. M. Gounelle[1,2], F. H. Shu[3], H. Shang[4], A. E. Glassgold[5], K. E. Rehm[6] and T. Lee[7]. [1]Université Paris XI-CSNSM. Bâtiment 104, 91 405 Orsay, France (gounelle@csnsm.in2p3.fr). [2]Department of Mineralogy, The Natural History Museum, London, UK. [3]National Tsinghua University, Hsinchu, Taiwan (shu@mx.nthu.edu.tw). [4]Institute of Astronomy and Astrophysics, Academia Sinica, Taipei, Taiwan (shang@asiaa.sinica.edu.tw). [5]Department of Astronomy, University of California, Berkeley, CA 94720, USA (aeg@astro.berkeley.edu). [6]Physics Division, Argonne National Laboratory, Argonne IL 60431, USA (rehm@anph11.phy.anl.gov). [7]Institute of Earth Science, Academia Sinica, Taipei 115, Taiwan (typhoon@asiaa.sinica.edu.tw).

Introduction: Radionuclides with half-lives of the order of the Ma were present in the accretion disc when the components of chondrites, Calcium-Aluminium-rich Inclusions (CAIs) and chondrules, formed (see [1] for a recent review). Some short-lived radioanuclides such as ^{10}Be, ^{26}Al, ^{41}Ca and ^{53}Mn were present in early Solar System at levels above expectations from the continuous galactic nucleosynthesis, requiring therefore a special, last-minute, explanation for their origin (e.g. [1]). Two models have been proposed for the origin of these extinct short-lived radionuclides. The external stellar model stipulates that they were made in a supernova or an AGB star, and injected within the collapsing molecular cloud core that would eventually lead to the formation of our Sun, meteoritic components and planets (e.g. [2]). Alternatively, the internal irradiation model stipulates that short-lived radionuclides have been produced via *in situ* irradiation of accretion disc gas and/or dust by energetic particles (protons, ^{4}He, ^{3}He) accelerated by the protosun (e.g. [3-5]). Distinguishing between these two models has critical implications for low-mass star formation theories and the origin of chondrites.

Since last year's LPSC, two recent experimental findings shed a new light on the origin of short-lived radionuclides and have urged us to revisit the irradiation model we proposed for the origin of short-lived radionuclides [3, 4, 6] in the context of the x-wind model [7]. In some rare hibonites from the CM2 chondrites, Mahras et al. [8] detected the past presence of ^{10}Be while the decay product of ^{26}Al is conspicuously absent. This decoupling between ^{10}Be and ^{26}Al was interpreted as contradicting irradiation models that simultaneously produce ^{10}Be and ^{26}Al. At this conference, Chaussidon et al. [9] make a strong case for the presence of ^{7}Be in the early Solar System at a level ^{7}Be/^{9}Be = (4.9 ± 1.3) x 10^{-3}. This value is two orders of magnitude smaller than the one presented previously [10], and that we discussed last year [11].

In this paper, we explore the possibility of bringing this new experimental data set in a coherent way within the framework of our irradiation model [3, 4, 6]. Compared to our 2001 calculations, no parameters were changed. Since the only modifications are the addition of ^{7}Be to the list of calculated yields, and the use of better constrained nuclear cross sections, we refer the reader to our previous work for details of the irradiation model.

Results: Because of its short half-life (53 days) compared to typical irradiation timescales varying between a few years to a few 10s of years, ^{7}Be yields need to be calculated at saturation. In other words, ^{7}Be/^{9}Be = f_7 x τ instead of, for example, ^{10}Be/^{9}Be = f_{10} x t_{irr}, where f_7 and f_{10} are the production rates of ^{7}Be and ^{10}Be respectively, τ is the mean-life of ^{7}Be and t_{irr} the irradiation time. For ^{7}Be we consider p, ^{3}He, ^{4}He channels on ^{16}O. Cross sections are taken from the compilation of [12] and completed with simulations. For the cross sections ^{24}Mg(^{3}He,p)^{26}Al and ^{4}He(^{16}O,x)^{10}Be, we used respectively the new measurement of [13] and previoulsy overlooked experimental data [14].

Figure 1 shows the calculated yields of short-lived radionuclides. We have distinguished between the two classes of flares occurring within the modern Sun: impulsive and gradual flares corresponding to ^{3}He- and proton-rich events respectively [15]. The spectral parameters, as well as the relative abundance of cosmic-rays are identical to [3], i.e. p = 4, ^{3}He/p = 0.3, ^{4}He/p = 0.1 for impulsive flares and p = 2.7, ^{3}He/p = 0, ^{4}He/p = 0.1 for gradual flares, with p being defined as $dN = E^{-p} dE$, where N is the number flux of protons. We are in the case 2d of [3], where the core size distribution of protoCAIs range from 50 μm to 2.5 cm, similar to natural CAIs, and *M*, the effective number of passage of protons in the irradiation zone is 1.6.

Without changing any parameters, the yield of ^{7}Be is in a very good agreement with the value found by [9]. The impulsive flares yield a value ^{7}Be/^{9}Be = 7.5 x 10^{-3} to be compared to the experimental value ^{7}Be/^{9}Be = (4.9 ±1.3) x 10^{-3} [9]. Gradual flares produce an even better agreement, with ^{7}Be/^{9}Be = 6.2 x 10^{-3}. Given the uncertainties discussed below, these differences between impulsive and gradual flares are insignificant. The main difference between the two types of flares is the ability of impulsive flares to produce the complete set of short-lived radionuclides at the meteoritic level.

Discussion: Because of its very short half-life (53 days) compared to the evolutionary timescales of pro-

tostars (10^5-10^6 yr), the presence of ^{7}Be in CAIs is a smoking gun for evidence of in situ irradiation. Unless CAIs themselves formed outside the Solar System, it is not possible to make ^{7}Be at a stage anterior to the CAI formation without having ^{7}Be decay to negligible levels. Impulsive flares that can account for the abundance of ^{10}Be, ^{26}Al, ^{41}Ca and ^{53}Mn, can reproduce, within errors the observed abundance of ^{7}Be in CAIs.

The rare CAIs containing ^{10}Be and no ^{26}Al can be accounted for by gradual flares that have the property of producing high levels of ^{10}Be while underproducing ^{26}Al and ^{41}Ca (see Figure 1). Gradual flares are 100 times less abundant in the contemporary Sun than impulsive flares [15] in agreement with the rarity of FUN-like CAIs relatively to "normal" CAIs. The overproduction of ^{10}Be by these flares (see Figure 1) can be accounted for by a combination of shorter exposure ages and lower luminosity for rare gradual flares in protostars. Because X-ray observations of protostars are still in their infancy, we cannot at the present time distinguish between the two possibilities. We note that a shorter exposure age is compatible with the origin of FUN-like CAIs proposed by [4]. According to these authors, FUN-like CAIs have retained some isotopic anomalies because they spent only short times in the reconnection ring where isotopic homogeneisation occurs [3].

We did not try to adjust our parameters (proton spectral shape, helium nuclei abundances...) to obtain a perfect match (see Figure 1) between our model and the experimental value. Indeed, the large uncertainties, mainly on the nuclear cross sections, but also on the cosmic-ray physics of protostars would make this attempt meaningless. We feel satisfied that our model can reproduce, the large diversity of new experimental data within a factor of a few. This is done with reasonable input parameters as the high abundance of ^{3}He nuclei is now well established for impulsive flares [16], and since we scale our yields to the X-ray luminosity of protostars [17].

Conclusions: The wealth of new experimental data can be accounted for by our irradiation model. We note that we calculated in 2003 a value ^{7}Be/^{9}Be ~ 3 x 10^{-3} [11], close to the value found experimentally some months later. Our model emphasizes the importance in distinguishing between impulsive and gradual flares. While impulsive flares can account for the distribution of short-lived radionuclides within normal CAIs, the rare gradual flares can account for the distribution of short-lived radionuclides in rare FUN-like CAIs. In addition, we will discuss at the conference the implications for our model of the discovery of ^{60}Fe in ordinary chondrites [18].

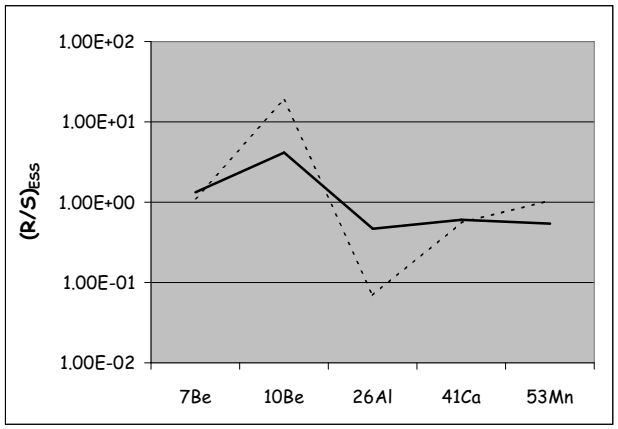

Figure 1: Yields of radionuclides normalised to their Early Solar System (ESS) values. Continuous line and dotted lines are impulsive and gradual flares respectively.

References: [1]S.S. Russell, M. Gounelle and R. Hutchison, *Phil. Trans. R. Soc. Lond. A* 359 (2001) 1991-2004. [2]M. Busso, R. Gallino and G.J. Wasserburg, *Publications of the Astronomical Society of Australia* 20 (2003) 356-370. [3]M. Gounelle, et al., *Astrophysical Journal* 548 (2001) 1051-1070. [4]T. Lee, et al., *Astrophysical Journal* 506 (1998) 898-912. [5]I. Leya, A.N. Halliday and R. Wieler, *Astrophysical Journal* 594 (2003) 605-616. [6]F.H. Shu, et al., *Astrophysical Journal* 548 (2001) 1029-1050. [7]F.H. Shu, et al., *Science* 277 (1997) 1475. [8]K.K. Marhas, J.N. Goswami and A.M. Davis, *Science* 298 (2002) 2182-2185. [9]M. Chaussidon, F. Robert and K.D. McKeegan, *Lunar Planet. Sci. Conf.* 35 (2004) This conference. [10]M. Chaussidon, F. Robert and K.D. McKeegan, *Meteoritics Planet. Sci.* 37 (2002) A31. [11]M. Gounelle, et al., *Lunar Planet. Sci. Conf.* 34 (2003) #1833. [12]Landolt-Börnstein, Springler-Verlag, 1994. [13]C. Fitoussi, et al., *Lunar Planet. Sci. Conf.* 35 (2004) This Conference. [14]H.-J. Lange, et al., *App. Radiat. Isot.* 46 (1995) 83-112. [15]D.V. Reames, *Rev. Geophys. Supp.* 33 (1995) 585-589. [16]J. Torsti, et al., *Astrophysical Journal* 573 (2002) L59-L63. [17]E.D. Feigelson, G.P. Garmire and S.H. Pravdo, *Astrophysical Journal* 584 (2002) 911-930. [18]S. Tachibana and G.R. Huss, *Astrophysical Journal* 588 (2003) L41-L44.

A NANOSIMS STUDY OF IRON-ISOTOPIC COMPOSITIONS IN PRESOLAR SILICON CARBIDE GRAINS. K. K. Marhas[1], P. Hoppe[1], and A. Besmehn[1,2], [1]Max-Planck-Institute for Chemistry, Cosmochemistry Department, D-55020 Mainz, Germany (kkmarhas/hoppe@mpch-mainz.mpg.de), [2]Research Centre Jülich, Central Department of Analytical Chemistry, D-52425 Jülich, Germany (a.besmehn@fz-juelich.de).

Introduction: Silicon carbide (SiC) is the best studied presolar mineral phase [1-3]. It is now well established that most of the presolar SiC (mainstream grains and the minor type Z and Y grains) originate from low-mass (1-3 $M_{\odot}$) asymptotic giant branch (AGB) stars. Also type II supernovae (SN) are believed to have contributed to the population of presolar SiC (X grains). Although low in abundance (about 1% of the SiC) the study of X grains has provided important insights into SN nucleosynthesis [e.g., 4, 5].

Only little isotopic information is available for the astrophysically diagnostic element Fe. To date Fe-isotopic compositions were measured for 4 mainstream grains, 9 unclassified grains, and 3 X grains by RIMS [6, 7]. These studies led to surprising results as $^{54}Fe/^{56}Fe$ ratios in mainstream (and unclassified) grains are distinctly lower than solar, having an average $\delta^{54}Fe$ of -130 ‰. Also $^{57}Fe/^{56}Fe$ ratios are mostly lower than solar, although the depletions in ^{57}Fe are less pronounced than those in ^{54}Fe. $^{58}Fe/^{56}Fe$ ratios, on the other hand, show a large scatter around the solar ratio. The lower than solar $^{54}Fe/^{56}Fe$ has been interpreted to be the imprint of Galactic chemical evolution (GCE) [6]. While two of the X grains have $^{54}Fe/^{56}Fe$ ratios in the range of mainstream grains, one X grain is enriched in ^{54}Fe by about 200 ‰. Excesses of several 100 ‰ (with large analytical uncertainties) are seen for ^{57}Fe and ^{58}Fe in all X grains [6].

In order to get additional information on the Fe-isotopic composition of presolar SiC we have measured Fe-isotopic ratios in 8 grains with the NanoSIMS 50 ion microprobe at MPI for Chemistry, Mainz.

Experimental: SiC grains separated from the Sahara 97166 enstatite chondrite [8] were dispersed on gold foils. Prior to the NanoSIMS measurements the sample was screened by low-mass resolution ion imaging for $^{30}Si/^{28}Si$ ratios with our Cameca IMS3f ion microprobe in order to locate the rare X grains. Four X grains identified by ion imaging were subsequently relocated in the NanoSIMS and measured together with 8 additional grains for C, N, and Si-isotopic compositions. Negative secondary ions of ^{12}C, ^{13}C, $^{12}C^{14}N$, $^{12}C^{15}N$, ^{28}Si, ^{29}Si, and ^{30}Si were measured in a combined multi-detection/peak-jumping mode using a defocussed (1-2 µm) Cs^+ primary ion beam of <1 pA.

Fe-isotopic ratios were measured in two of the X grains and in 6 grains of other types. Positive secondary ions of ^{28}Si, ^{52}Cr, ^{54}Fe, ^{56}Fe, and ^{57}Fe were analyzed in a combined multi-detection/peak-jumping mode with a defocussed (~2 µm) primary O^- beam of ~10 pA. ^{58}Fe was not included in the measurements because of its low isotopic abundance (0.31 %). High-resolution ion images, acquired with a focussed O^- primary ion beam (~300 nm), were taken in order to check for possible contributions of Fe contamination to the grains's intrinsic Fe.

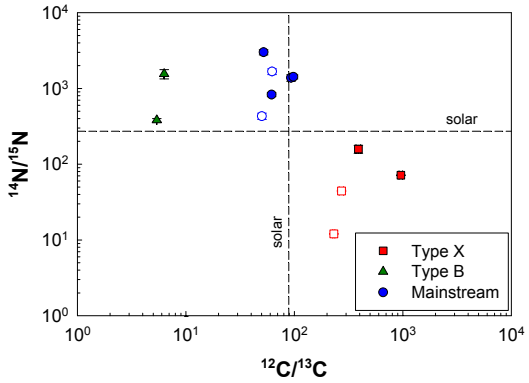

Figure 1. C- and N-isotopic compositions of presolar SiC grains from the Sahara 97166 enstatite chondrite. Errors are 1σ. Filled symbols: Measured for Fe-isotopic composition; open symbols: not measured for Fe-isotopic composition.

Results: According to C-, N-, and Si-isotopic compositions, 2 of the SiC grains analyzed for Fe are of type B, 4 of the mainstream type, and 2 of type X (Table 1, Fig. 1). Fe/Si ratios are between $4.7x10^{-4}$ and 0.016 in the type B and mainstream grains, and around 0.01 in the X grains. In the mainstream grain SiC#13 there is a clear indication of Fe contamination as evidenced from a pronounced difference in the Si and Fe ion images (Fig. 2). Without this grain, Fe/Si ratios range up to 0.002 in B and mainstream grains, consistent with what was observed in previous studies [9]. The Fe/Si ratios in the X grains are higher by a factor >10 than those previously studied [10]. However, at least for grain SiC#422-1 this seems to be an intrinsic feature because Fe is homogeneously distributed within the grain (Fig. 2).

The $^{54}Fe/^{56}Fe$ and $^{57}Fe/^{56}Fe$ ratios of the B and mainstream grains as well as of X grain SiC#294-3 are normal within 2σ (Fig. 3). The mass-weighted average of $\delta^{54}Fe$ in the B and mainstream grains (w/o SiC#13) is $\delta^{54}Fe = -34 \pm 31$ ‰ and $\delta^{57}Fe = 9 \pm 24$ ‰. The only resolvable anomalies are seen for $^{54}Fe/^{56}Fe$ and $^{57}Fe/^{56}Fe$ in X grain SiC#422-1 (Fig. 3). But even here,

the anomalies are relatively small with excesses in ^{54}Fe and ^{57}Fe of only 30-40 ‰.

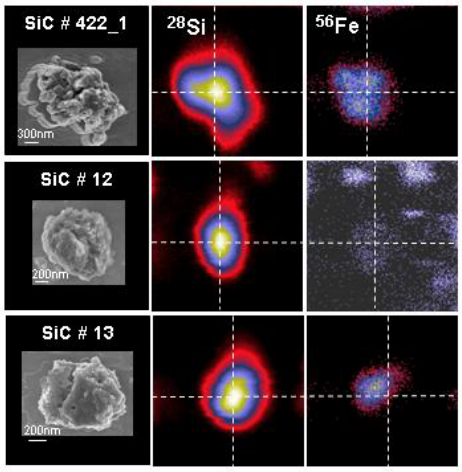

Figure 2. SEM and ^{28}Si and ^{56}Fe ion images of X grain SiC#422-1, and mainstream grains SiC#12 and SiC#13. Field of view is 5 x 5μm^2.

Discussion: The ^{54}Fe/^{56}Fe data of our B and mainstream grains fall at the upper end of the ratios measured by [6, 7] for mainstream grains. In AGB stars ^{54}Fe and ^{56}Fe are consumed by n-captures in the He intershell and the envelope abundances of these two isotopes change only marginally during the third dredge-up events. Contrary, large amounts of ^{57}Fe are produced by n-capture in the He intershell and the third dredge-up will increase the envelope ^{57}Fe/^{56}Fe ratio significantly [6]. The average δ^{54}Fe and δ^{57}Fe values of our B and mainstream grains are roughly compatible with model predictions (δ^{54}Fe ~0, δ^{54}Fe = 50-150 ‰) for 1.5-5 $M_\odot$ AGB stars of solar metallicity and initially solar Fe-isotopic composition [6]. A better match, however, is achieved for $\delta^{54}Fe_{ini}$ ~ -25 ‰ and $\delta^{57}Fe_{ini}$ ~ -90 ‰. In terms of GCE this would mean that ^{54}Fe and ^{57}Fe were depleted relative to solar isotopic abundances at the time the SiC grains formed.

In the different zones of type II SN Fe-isotopic compositions vary over many order of magnitudes. It was shown that the isotopic compositions of many elements in X grains can be satisfactorily explained if matter from the Si/S-, He/C, and He/N zones is mixed in variable proportions [4]. Small contributions from the interior Ni zone, which probably provides the ^{44}Ti seen in many X grains [4], will have a strong impact on the Fe-isotopic ratios because of very high concentrations of ^{56}Fe and its radioactive progenitors. In view of the large variations expected for Fe-isotopic ratios in different SN zones, the close-to-normal ratios in the X grains of this study are surprising. Nevertheless, the Fe-isotopic signature of X grain SiC#422-1 is qualitatively consistent with that observed by [6] for one of their X grains and can be qualitatively understood in terms of the 15 $M_\odot$ type II SN model of [11] by mixing matter from the Si/S, He/C, and He/N zones, although the observed excess in ^{54}Fe falls short of that expected for mixtures that can reproduce the Si-isotopic signature of SiC#422-1 (see Fig. 10 in [4]).

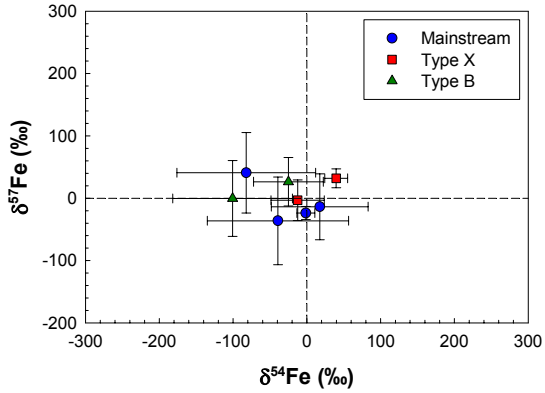

Figure 3. Fe-isotopic compositions of presolar SiC grains from the Sahara 97166 enstatite chondrite. Errors are 1σ.

Acknowledgements: We thank J. Huth for his help with the SEM and E. Gröner for technical assistance.

References: [1] Zinner E. (1998) *Ann. Rev. Earth Planet. Sci.*, 26, 147. [2] Hoppe P. and Zinner E. (2000) *JGR*, 105, 10371. [3] Nittler L. R. (2003) *EPSL*, 209, 259. [4] Hoppe P. et al. (2000) *MAPS*, 35, 1157. [5] Pellin M. et al. (1999) *LPSC*, 30, abstr. #1969. [6] Davis A. M. et al. (2002) *LPSC*, 33, abstr. #2018. [7] Tripa C. E. et al. (2002) *LPSC*, 33, 1975. [8] Besmehn A. (2001) *PhD. thesis*, Universität Mainz. [9] Amari S. et al. (1995) *Meteoritics*, 30, 679. [10] Hoppe P. et al. (2001) *ApJ*, 551, 478. [11] Woosley S. E. and Weaver T. A. (1995) *ApJS*, 101, 181.

Table 1. C-, N-, Si-, and Fe-isotopic compositions and Fe/Si ratios in presolar SiC grains from Sahara 97166.

Grain	Type	δ^{29}Si (‰)	δ^{30}Si (‰)	^{14}N/^{15}N	^{12}C/^{13}C	δ^{54}Fe (‰)	δ^{57}Fe (‰)	Fe/Si x10^{-3}
SiC#12	Mainstream	-3 ± 4	3 ± 5	3003 ± 232	52.0 ± 0.4	-82 ± 94	41 ± 65	0.47
SiC#13	Mainstream	-16 ± 3	2 ± 3	1380 ± 137	93.1 ± 0.6	-1 ± 12	-24 ± 10	16.0
SiC#17	Mainstream	-12 ± 6	3 ± 7	1423 ± 87	98.1 ± 1.3	18 ± 66	-14 ± 53	4.7
SiC#408-7	Mainstream	48 ± 6	38 ± 8	828 ± 49	61.6 ± 0.7	-39 ± 96	-36 ± 70	1.24
SiC#10	B	34 ± 5	26 ± 6	381 ± 20	5.4 ± 0.02	-101 ± 81	-0 ± 61	1.91
SiC#14	B	-8 ± 5	24 ± 6	1552 ± 216	6.3 ± 0.02	-25 ± 47	26 ± 39	0.65
SiC#294-3	X	-336 ± 10	-491 ±11	158 ± 19	389 ± 19	-13 ± 36	-3 ± 33	14.6
SiC#422-1	X	-313 ± 5	-498 ± 5	71 ± 1	959 ± 36	40 ± 16	32 ± 15	11.5